Wettability of partially suspended graphene

Thierry Ondarçuhu, Vincent Thomas, Marc Nuñez, Erik Dujardin, Atikur Rahman, Charles T. Black, Antonio Checco

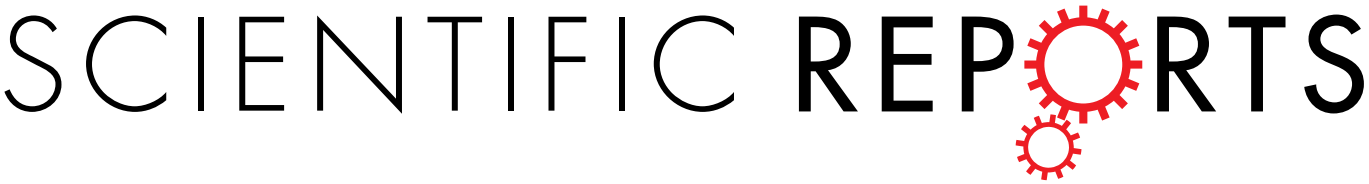

OPEN

Wettability of partially suspended graphene

Thierry Ondarçuhu[1], Vincent Thomas[1], Marc Nuñez[1], Erik Dujardin[1], Atikur Rahman[2], Charles T. Black[2] & Antonio Checco[3]

Received: 30 December 2015
Accepted: 22 March 2016
Published: 13 April 2016

The dependence of the wettability of graphene on the nature of the underlying substrate remains only partially understood. Here, we systematically investigate the role of liquid-substrate interactions on the wettability of graphene by varying the area fraction of suspended graphene from 0 to 95% by means of nanotextured substrates. We find that completely suspended graphene exhibits the highest water contact angle (85° ± 5°) compared to partially suspended or supported graphene, regardless of the hydrophobicity (hydrophilicity) of the substrate. Further, 80% of the long-range water-substrate interactions are screened by the graphene monolayer, the wettability of which is primarily determined by short-range graphene-liquid interactions. By its well-defined chemical and geometrical properties, supported graphene therefore provides a model system to elucidate the relative contribution of short and long range interactions to the macroscopic contact angle.

Graphene, the one-atom thick, two-dimensional carbon allotrope, has received significant attention owing to its extraordinary electronic, optical and mechanical properties[1]. Advanced coating applications of graphene may also benefit from its high mechanical and thermal stability, excellent chemical resistance and impermeability to gases[2]. Yet, the full technological potential of graphene coatings still requires better understanding of how the atomic monolayer alters the physicochemical properties of the underlying substrate. In particular, the extent of "wetting transparency" of graphene – i.e. transparency to chemical, van der Waals and electrostatic interactions between liquid and substrate atoms or molecules – remains a much debated question[3–7]. In principle, the wettability of graphene-coated solids should depend on graphene-liquid short range interactions but also on solid-liquid long range interactions[8,9]. An early study by Rafiee *et al.*[3] suggested that graphene coatings are "transparent" to wetting i.e. do not significantly alter the intrinsic wettability of apolar solids, which interact with water predominantly through van der Waals forces. Conversely, other authors[4–6,10] partially revised these conclusions by showing experimentally that graphene is only partially transparent (or "translucent") to wetting. Progress on this complex topic has been hampered by experimental shortcomings such as defects occurring during the growth and/or transfer of graphene on a substrate[5], as well as adventitious carbon contamination[10], both of which were shown to dramatically alter the intrinsic wettability of graphene and graphitic materials alike[11,12]. The theoretical description of graphene wetting phenomena is equally challenging because they are highly dependent on the model taken for the adsorbate-graphene interactions. For instance, the adsorption of water on graphene is not accurately reproduced by density functional theory (DFT) even when effects of dispersive interactions are taken into account[13,14]. Several Molecular Dynamics (MD) studies have modeled the wettability of graphene but their results depend quantitatively on the choice of the water−carbon interaction potentials[4,5,15,16], which are not known precisely. Nevertheless, MD as well as mean field approaches on flat[4,5,16] and rough[15] substrates are consistent with the partial wetting transparency of graphene observed in some experiments.

Despite considerable progress, a comprehensive and consistent understanding of water-graphene interactions is still lacking. Bridging this gap requires the characterization of the intrinsic wetting properties of a suspended graphene sheet in the absence of any interactions with the supporting substrate. However, this is experimentally challenging since capillary forces exerted by macroscopic drops on the graphene membrane may either tear it or fold it. Here, we circumvent this limitation by preparing graphene monolayers partially supported on nanopatterned silicon substrates over macroscopically large (cm^2) areas. The surface fraction of suspended graphene is varied from 0% to approximately 95% by controlling the morphology of the textured substrate, which allows quantifying the effect of water-substrate interactions on the wettability of graphene. Further, we develop a novel

[1]Nanosciences group, CEMES-CNRS, 29 rue Jeanne Marvig, Toulouse 31055, France. [2]Center for Functional Nanomaterials, Brookhaven National Laboratory, Upton, NY 11973, USA. [3]Condensed Matter Physics and Materials Science Department, Brookhaven National Laboratory, Upton, NY 11973, USA. Correspondence and requests for materials should be addressed to T.O. (email: ondar@cemes.fr) or A.C. (email: checco@bnl.gov)

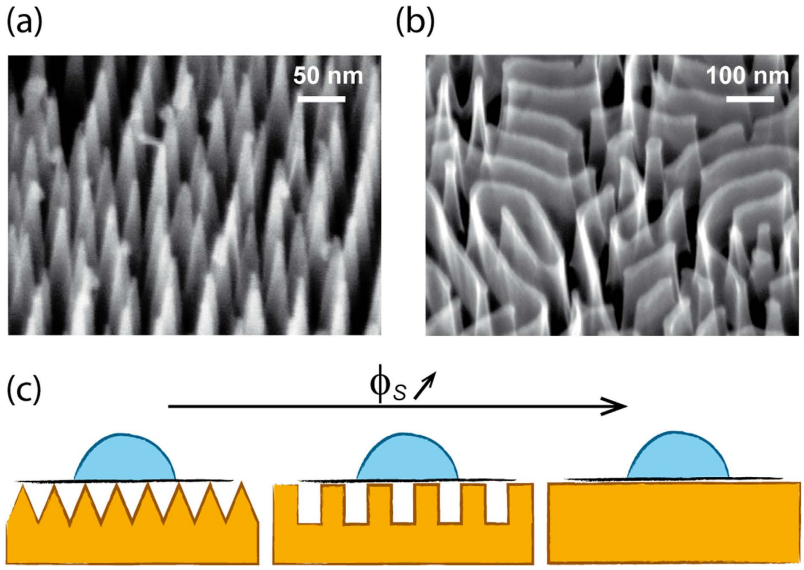

Figure 1. (**a**) SEM micrograph of a nanopatterned substrate with conical tips and spacing of 50 nm. (**b**) SEM micrograph of a substrate with 16 nm-wide grooves and a 70 nm period. (**c**) Sketch of the experiment.

procedure for transferring graphene to a solid support that obviates the irreversible contamination associated to polymer-assisted transfer. The water contact angle on both fully supported and partially suspended graphene depends marginally on the chemical nature of the substrate and the suspension fraction, albeit suspended monolayers are slightly more hydrophobic than supported ones. We show that the wettability of graphene is dictated primarily by water-graphene interactions and to a much lesser extent by water-substrate interactions. By its well-defined chemical and geometrical properties, supported graphene therefore provides a model system to elucidate the relative contribution of short and long range interactions to the macroscopic contact angle[8,9].

Results

Fabrication and characterization of suspended graphene layers. In order to tailor the fraction of suspended graphene, we have fabricated large area (~1 cm^2), nanopatterned silicon surfaces with uniform feature size and spacing on a 10-nm length scale using block copolymer self-assembly and plasma etching (Fig. 1)[17]. Tapered conical structures with either sharp (width $w \sim 5\,nm$) or flat ($w \sim 15\,nm$ to $w \sim 30\,nm$) tips were obtained using a block-copolymer mask with cylindrical morphology and by varying the vertical and lateral etching rates (Fig. 1a). Fingerprint patterns of grooves and ridges (size w~12 nm to w~20 nm at the top) were obtained using a block copolymer mask with lamellar morphology (Fig. 1b). A precise control over the texture morphology allowed varying the solid areal fraction at the top of the texture ϕ_S from approximately 5–80%, thereby making these substrates ideally suited to fundamental studies of wetting of suspended graphene by water (Fig. 1c). Moreover, we performed surface functionalization to obtain patterned substrates with either hydrophilic or hydrophobic properties (see Methods for details).

Supported and partially suspended graphene monolayers were transferred from copper foils bearing graphene grown by chemical vapor deposition (CVD)[18,19]. A most common procedure for transferring graphene from copper to another supporting material starts by stabilizing the supported graphene monolayer with a thick layer of polymer (e.g. poly-methyl methacrylate, PMMA)[3–5,10]. Although this method allows transferring large (~1 m^2) graphene films without compromising its mechanical integrity[20,21], it leads to irreversible polymer contamination of the graphene surface[22,23], thereby altering its intrinsic wettability. In order to circumvent this issue, we have developed a polymer-free transfer method sketched in Fig. 2a and described in detail in Methods section.

The quality of the layers transferred onto flat and nanopatterned silicon substrates was assessed by optical microscopy, atomic force microscopy (AFM), Raman spectroscopy and scanning electron microscopy (SEM). The overall integrity of the graphene layer deposited on flat silicon is preserved during the transfer procedure leaving large areas available for contact angle measurements. However, contrary to polymer-assisted transfer methods, the graphene monolayer exhibits wrinkles most likely caused by surface tension forces acting on the floating layer after the copper foil is etched away (Fig. 2b and Supplementary Fig. SI1). These wrinkles appear as darker, narrow lines (~100 nm-wide) in both SEM and optical microscopy images (Fig. 2b) covering 6-8% of the graphene surface. Moreover, graphene pinholes were observed with diameters of a few micrometers covering about 1-2% of the graphene surface.

Graphene monolayers transferred onto nanopatterned substrates remain suspended without sagging significantly into the voids, regardless of the porosity of the texture, as shown in Fig. 3 (see Supplementary Section SI2 for further details). AFM inspection reveals that the root mean square (rms) roughness of the graphene layer deposited on a nanocone texture is less than 0.4 nm between wrinkles (see inset of Fig. 3d). This remarkable result is understood by considering the large elastic bending energy required to conform the graphene sheet to

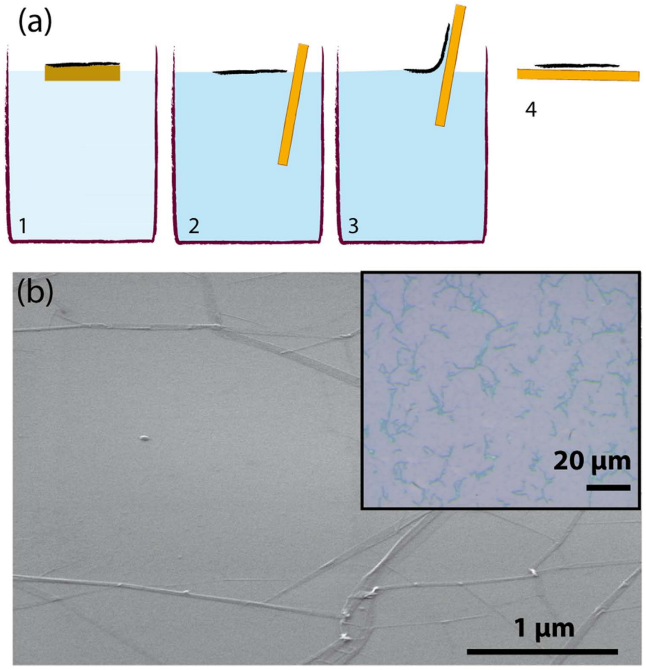

Figure 2. (**a**) Scheme of the transfer method: (1) the copper foil supporting the graphene is etched by an ammonium persulfate solution leaving a floating monolayer (2); the graphene foil is then scooped on a glass slide and redeposited on a water surface for rinsing (not shown); the monolayer is then scooped out on the substrate (3) and dried (4). (**b**) SEM image of a graphene layer deposited on a flat SiO_2/Si substrate; inset: optical micrograph of the layer; in both images wrinkles appear as darker lines.

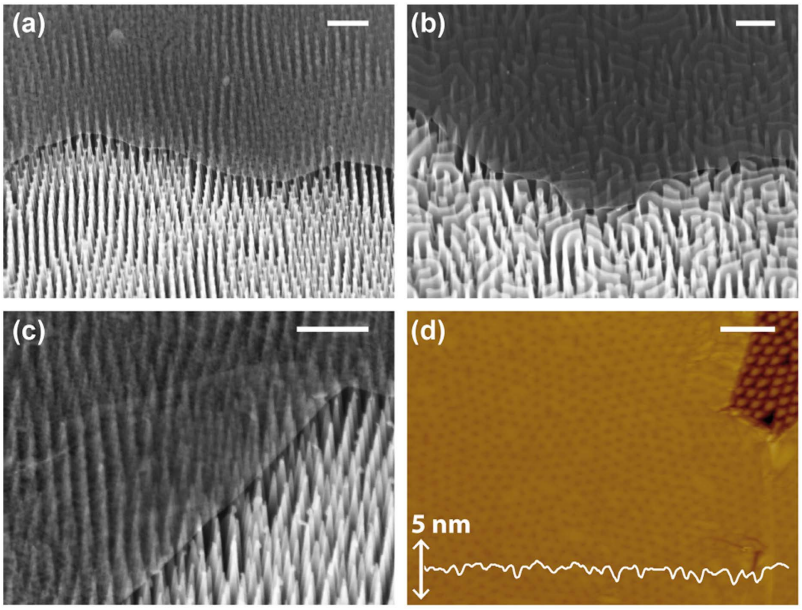

Figure 3. (**a**–**c**) SEM images of graphene layers deposited on textures composed of tapered cones with flat tips, grooves, and tapered cones with sharp tip, respectively; (**d**) AFM image of graphene layer on a conical texture where the white line represent a cross-sectional profile. Scale bar is 200 nm.

textures with extremely small period (~50 nm) and high aspect ratio. It is consistent with a recent study showing that graphene remains suspended atop post arrays if the inter-post distance is less than a critical length approximatively equal to 250 nm[24]. At the micrometer scale, the structure of the suspended monolayers exhibits a pattern of folds similar in aspect and area fraction coverage to that observed on graphene transferred on flat substrates. However, a significantly larger pinhole density (~8%) was observed on monolayers deposited on sharp nanocone textures with a substrate fraction $\phi_s < 15\%$ (see Supplementary Fig. SI2). On textured substrates, the occasional

presence of small cracks connecting series of posts is also observed. We hypothesize that these cracks are formed by releasing the strain induced by capillary forces during the drying of the textured substrates.

The efficiency of the graphene transfer on hydrophobic textures, is smaller partly because of the turbulences occurring during the addition of isopropanol in water, which sometimes tear the graphene layer into fragments too small for contact angle measurements. The transfer of graphene on conical textures systematically leads to fragmented layers which are only partially suspended and cannot be used for contact angle measurements.

While our graphene monolayers are free of polymer contamination, adventitious carbon readily adsorbs on graphene exposed to ambient air and alters its intrinsic wettability[10]. In order to remove these contaminants, the samples were systematically annealed at high temperature under a continuous flow of reductive Ar/H_2 atmosphere (see Methods)[22,23,25,26]. We observed that this process effectively removes the adsorbates on the commecial CVD-grown graphene samples. The efficiency of the cleaning protocol was assessed by high resolution transmission electron microscopy imaging and diffraction while Raman spectroscopy gave strong indications of a single monolayer (see Supplementary Section SI3).

The protocol for reproducible contact angle measurement was optimized on graphene monolayers transferred onto flat silicon dioxide from three different commercial CVD-grown graphene sources (see Supplementary Section SI4). Advancing and receding contact angles were measured on several graphene regions, immediately after the reductive annealing and for a few hours afterwards. The quality of the layers transferred onto flat and nanopatterned silicon substrates was assessed[10,11]. Interestingly, the advancing contact angle is very reproducible (standard deviation $<1°$) whereas receding contact angle is more sensitive to defects (standard deviation $>9°$)[5]. Consequently, we characterized the intrinsic properties of graphene layers by measuring advancing contact angle values obtained within ten minutes after the annealing process.

Wetting properties of the bare substrates. In order to investigate the influence of a graphene layer on the wetting properties of a substrate, we first characterized the wettability of the bare nanopatterned substrates. The measurements were performed on bare parts of the samples supporting graphene to ensure that both situations (with and without graphene monolayer) were subject to identical surface treatments and that wettability differences can therefore be attributed to the graphene influence. In particular, the Ar/H_2 annealing significantly modifies the wettability of flat SiO_2 substrates. We have found that the flat silicon samples were completely wet by water after piranha cleaning ($\theta_{SiO_2}^{native} = 0°$) but became less hydrophilic after annealing, $\theta_{SiO_2}^{anneal} = 55° \pm 4°$. Conversely, the wettability of the flat fluorinated SiO_2 samples ($\theta_{FLSiO_2} = 105° \pm 1°$) remained unchanged after annealing suggesting that the surface treatment did not significantly compromise the structural integrity of the silane coating. The advancing contact angles of the hydrophilic and hydrophobic nanopatterned surfaces, denoted as θ_S^{philic} and θ_S^{phobic} respectively, are reported in red in Fig. 4 as a function of the solid area fraction ϕ_s (red filled and red open circles respectively). These results show that the surface roughness enhances either the hydrophilic or the hydrophobic character of the substrates. For the sharper structures ($\phi_S < 10\%$), the contact angle was found to be a few degrees for hydrophilic substrates whereas it reached 165° for the hydrophobic ones, typical of super-hydrophilic and super-hydrophobic surfaces[17], respectively. Optical images of the contact line region revealed that, on hydrophilic nanopatterned surfaces, a wetting film extended from 10 to 100 microns ahead of the contact line, depending on the surface texture. The film appeared bright close to the contact line and dark close to the leading edge. We hypothesize that the film forms through the spontaneous impregnation of the textures with water[27]. The film color variation reflects changes in thickness; the film is thick enough to cover the texture completely in the region close to the contact line, but only partially near leading edge. This "hemiwicking" occurs when the contact angle on the walls is smaller than a critical value defined by $\cos\,\theta^* \approx 1/r$ where r is the roughness ratio[27]. Our textured samples exhibit spontaneous wicking owing to their relatively high roughness ($r = 5 - 10$), and intrinsic hydrophilicity ($\theta_{SiO_2}^{anneal} = 55°$ on annealed SiO_2). Conversely, no such film was observed ahead of the droplet contact line on hydrophobic textures. In this case, wicking is suppressed by the surface hydrophobicity ($\theta_{SiO_2}^{FL} = 105°$ on fluorinated SiO_2) and the droplet remains suspended on the texture.

Based on these observations, we have modeled the contact angle of wettability θ_S of the bare patterns, denoted as θ_S using the Cassie-Baxter (CB) equation[28].

$$\cos\,\theta_S = \phi_S\,\cos\,\theta_T + (1 - \phi_S)\cos\,\theta_V \quad (1)$$

where θ_T is the contact angle on the textured material, and θ_V the contact angle on the medium filling the texture voids, i.e. water ($\theta_V = 0°$) or air ($\theta_V = 180°$) for the hydrophilic and hydrophobic textures, respectively. The CB model is plotted against the data in Fig. 4a using the experimental values $\theta_T = 55°$, 105° for the hydrophilic (solid green line) and hydrophobic (green dashed line) pattern, respectively. The good agreement between theory and experiment suggests that the CB model describes adequately the wetting of the whole range of complex composite surfaces studied here.

Wettability of partially suspended graphene monolayers. Next, we measured the contact angle θ_{GS} of water on the graphene layers transferred on the same nanostructures. On hydrophilic substrates, the optical observation of the droplets revealed features similar to the ones obtained on bare substrates resulting from the liquid impregnation of the textured surface beneath the graphene layer ahead of the contact line (Fig. 4b). Evaporation or removal of the droplet with the same syringe used for liquid dispensing demonstrated that the layer below the droplet is also filled with liquid. Under these conditions, the measured contact angle thus reflects the wettability of a graphene layer partially suspended on water, as schematized in the inset of Fig 4b. This contact angle was found to decrease very slightly with decreasing ϕ_s ranging from $\theta_{GS}^{philic} = 69° \pm 1°$, the value obtained on flat SiO_2 substrates, to $\theta_{GS}^{philic} = 67° \pm 2°$ for textures with $\phi_s < 15\%$(blue filled circles in Fig. 4a). However, a

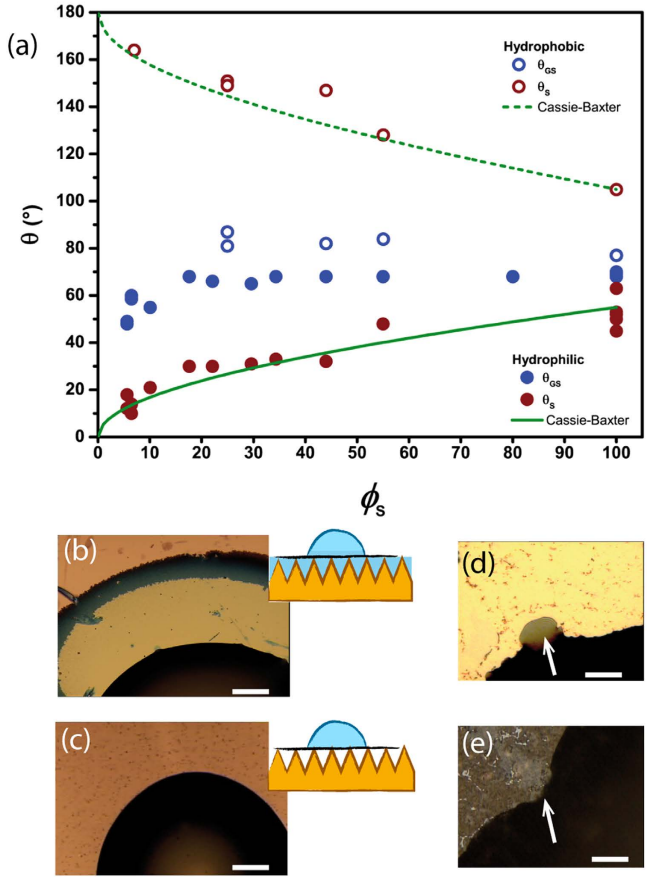

Figure 4. (**a**) Contact angles versus solid area fraction, ϕ_S, for bare hydrophilic (filled red circles), bare hydrophobic (hollow red circles), graphene-coated hydrophilic (filled blue circles), and graphene-coated hydrophobic substrates (hollow blue circles). Green solid and dashed lines represent the Cassie-Baxter contact angle for bare hydrophilic and hydrophobic substrates, respectively. (**b**,**c**) Top-view optical image of a water drop on a graphene coated hydrophilic and hydrophobic nanotexture, respectively, where the insets depict the wetting conditions schematically (scale bar = 100 μm). (**d**,**e**) Close up view of contact line distortions on a graphene coated hydrophilic and hydrophobic nanopatterned substrates, respectively, where arrows mark the defect location (scale bar = 10 μm).

significantly lower contact angle in the range $49° \leq \theta_{GS}^{philic} \leq 60°$ was found for sharp conical structures ($\phi_s < 15\%$).

The same experiments were performed on the hydrophobic substrates, where the weak adhesion of graphene onto fluorinated nanopatterned substrates occasionally resulted in graphene lifting off from the surface to wrap the droplet during contact angle measurements[29,30]. This issue, combined with the difficulty of transferring graphene to substrates with $\phi_S < 25\%$, resulted in a smaller number of reliable measurements on hydrophobic samples than on hydrophilic ones. Optical imaging of water droplets deposited on graphene supported by hydrophobic textures showed that the liquid does not spread ahead of the contact line (Fig. 4c) or beneath the graphene layer. This was due to the super-hydrophobic properties of the supporting substrate, which led to a water droplet on a graphene layer partially suspended on air as sketched in Fig. 4c. The contact angle measurements are reported in Fig. 4a in open blue circles. Similarly to the case of graphene supported by hydrophilic textures, no strong dependence on ϕ_S is observed. The average contact angle, was found to increase slightly from $\theta_{GS}^{phobic} = 77° \pm 1°$ on a flat fluorinated substrate to $\theta_{GS}^{phobic} = 83.5° \pm 2.5°$ on hydrophobic patterns with $\phi_S = 25\%$.

We can rule out the possibility that the weak dependence of $\theta_{GS}^{philic,\ phobic}$ on ϕ_s be due to defects in the graphene layer. In fact, the surface density of defects (either holes and cracks) in supported graphene sheets amounts to ~2% on flat supports and up to 8% on nanocone textures. These defects influence θ_{GS} depending on the wetting properties of the underlying substrate. On a superhydrophilic substrate, a hole in graphene locally creates a strong wetting defect, whereas on superhydrophobic substrates it gives rise to a strong non-wetting defect. These two types of defects are clearly visible in close-up viewgraphs of the contact line shown in Fig. 4d,e, respectively. Hence, the defects can in principle lead to an apparent decrease of θ_{GS}^{philic} (or increase of θ_{GS}^{phobic}) as a function of ϕ_S thereby mimicking the experimental results. We have modelled this effect using the Cassie-Baxter equation (see Supplementary Section SI5 for further details). Our calculations shows that defect densities up to 2% have a

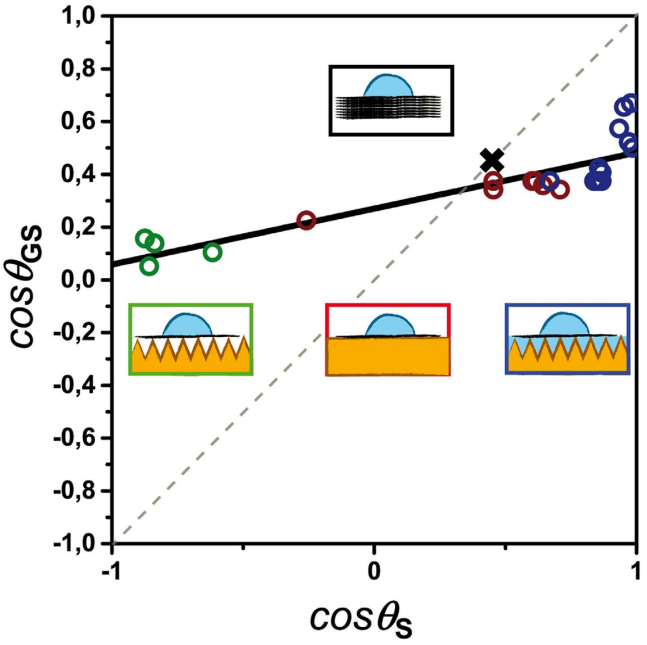

Figure 5. Plot of $\cos\theta_{GS}$ as a function of $\cos\theta_S$ for the three different systems schematized in the above insets: fully supported graphene in red, partially suspended on air in green and partially suspended on water in blue. The solid black line is a linear fit of the experimental data. Grey dashed line is the $\cos\theta_{GS} = \cos\theta_S$ line whereas the black cross marks the experimental wetting angle on HOPG.

limited effect (less than 10%) on θ_{GS}. However, the 8% defect density of graphene supported by superhydrophilic samples ($\phi_S < 15\%$), may account for up to 30% of the decrease of θ_{GS} measured on these substrates.

The dependence of θ_{GS} on the composition of the supporting substrate therefore reflects changes in water-graphene-substrate interactions, rather than the spurious effect of graphene defects. An important finding of this work is that the wettability of graphene varies very little even when it is supported by materials with very different chemical composition such as air, water, silicon dioxide, and fluorinated silicon oxide. This implies that θ_{GS} is dictated, to a large extent, by water-graphene interactions and, to a lesser extent, by long range water-substrate interactions through the graphene layer.

These findings partially differ from the results of *Raj et al.* who reported no influence of the underlying (hydrophilic) substrate and from a study by Shih *et al.*[4] who found that graphene is opaque to wetting for hydrophobic substrates ($\theta_S > 90°$) but showed some degree of transparence for hydrophilic substrates ($30° < \theta_S < 90°$). A combined influence of graphene and underlying substrate was also shown[6,10] but not described quantitatively. The lack of consensus among these studies may stem from the choice of contact angle measurement methods (static contact angle is not as well-defined as advancing angle due to contact angle hysteresis) or from sample preparation, which does not systematically eliminate airborne contaminants.

Discussion

In order to relate quantitatively the observed wetting translucency of graphene to the underlying molecular interactions, we have plotted the cosine of the contact angle of supported graphene, $\cos\theta_{GS}$, as a function of the cosine of the contact angle on the bare substrates, $\cos\theta_S$. Indeed, $\cos\theta_{GS}$ is related to the water-graphene-solid effective interaction potential per unit area W_{WGS} through the Young-Dupré equation[31].

$$\gamma(1 + \cos\theta_{GS}) = -W_{WGS} \tag{2}$$

where γ is the surface tension of water. Figure 5 gathers the measurements performed on all the fabricated samples which were categorized in three types, namely supported graphene (red open dots), graphene partially suspended on air (green open dots) and water (blue open dots). Remarkably, the data show that all experimental results collapse on a straight line except for data points in a narrow region where $\cos\theta_S \cong 1$. The scattering of data in this region is likely due to the larger density of graphene defects on hydrophilic nanocone textures ($\phi_d \sim 8\%$).

A linear fit to the data (solid black line) allows extrapolating the water contact angle on two ideal cases: totally suspended graphene $\theta_G = 85° \pm 5°$ (for $\cos\theta_s = -1$), and graphene floating on water, $\theta_{GW} = 61° \pm 5°$ (for $\cos\theta_s = +1$). Our results are well described by recent mean field calculations of water wetting a flat graphene sheet suspended on a rough substrate assuming dispersive interactions[15]. Specifically, the experimental difference $\Delta\theta = \theta_{GW} - \theta_G = -24°$ is in close quantitative agreement with $\Delta\theta_{theory} \approx -18°$. Driskill *et al.*[16] have predicted a slightly smaller $\Delta\theta_{theory} \approx -10°$ when taking into account both dispersive and dipolar interactions.

The data presented in Fig. 5 are also consistent with the experimental wetting of freshly cleaved, highly oriented pyrolytic graphite (HOPG). Since this material is composed of stacked graphene layers, its wettability should not change with the addition of a graphene coating, leading to the relationship $\theta_{GS} = \theta_S$. Hence, the

contact angle of water on HOPG can be determined graphically as the intersection of the linear fit to the data with the $\cos\theta_{GS} = \cos\theta_S$ line (dashed line in Fig. 5). The value $\theta_{HOPG} = 70° \pm 5°$ obtained from Fig. 5 is in good quantitative agreement with the experimental $\theta_{HOPG} = 62{,}4° \pm 0{,}9°$ shown in Fig. 5 as the black cross (see also Experimental Section for details). Wettability of few layered graphene can also be deduced graphically from the data in Fig. 5 as detailed in the Supplementary Section SI6.

The linear relationship between $\cos\theta_{GS}$ and $\cos\theta_S$ can also be understood by writing the generalized Young-Dupré equation for water on the bare substrate: $\gamma(1+\cos\theta_s) = -W_{WS}$, water on graphene: $\gamma(1+\cos\theta_G) = -W_{WG}$, and water on supported graphene $\gamma(1+\cos\theta_{GS}) = -W_{WGS} = -W_{WG} - \alpha W_{WS}$, where W_{WS} and W_{WG} are the water-substrate and water-graphene effective interaction potentials per unit area and we have also assumed that W_{WGS} can be linearly decomposed as $W_{WGS} \cong W_{WG} + \alpha W_{WS}$. α represents a phenomenological "screening parameter" that quantifies the degree of graphene transparency such that $\alpha = 0$describes a perfectly opaque layer. Solving these equations for $\cos\theta_{GS}$ yields:

$$\cos\,\theta_{GS} = \alpha\ \cos\,\theta_S + \ \cos\,\theta_G + \alpha \tag{3}$$

A linear fit to the experimental data gives $\alpha = 0,21 \pm 0,03$, or $\alpha = 0,19 \pm 0,03$ when a 2% defect density is taken into account (see Supplementary Section SI5 for further details). This result indicates that graphene screens 81% of the water-substrate interactions compared to a direct contact and is consistent with estimations by mean field theory[32] leading to about 70% of interactions blocked by a graphene monolayer.

The origin of this screening effect is twofold. On the one hand, the intercalation of graphene between water and substrate increases the average distance between the water molecules and the substrate thereby lowering their interaction. In the case of van der Waals and dipole-dipole interaction the resulting effective interaction potential per unit area then scales as[31] $W \sim 1/d^2$. On the other hand, these long range water-substrate interactions are mediated by the graphene sheet. The screening caused by the increased water–substrate distance alone can be approximated as $\alpha = (d_{WS}/d_{WGS})^2$ where d_{WS} and d_{WGS} are the equilibrium distances between liquid and substrate in contact or separated by graphene, respectively. An estimate of the screening in the particular case of wetting of graphene on water where $d_{WGS} = 2d_{WS}$ yields $\alpha = 0{,}25$. This value is very close to the experimental result, suggesting that, at least for solids and liquids interacting solely through dispersive forces, the "screening effect" can be almost entirely understood as an increase of water-substrate separation upon inserting the graphene coating. Note that, in the general case, the estimation of α requires a precise knowledge of the water-graphene and substrate-graphene distances which both are theoretically calculated to be of the order of 3 Å[5,33,34].

The experimental value of α is smaller than the pure geometrical estimate, which indicates that a small but significant weakening of the water-substrate interactions may arise from the weak but non-zero electrostatic screening efficiency of the graphene layer[35].

Although these results can be understood qualitatively using continuum models of dispersive and dipolar interactions within a mean field approach, a rigorous quantitative description requires more sophisticated calculations based on DFT and molecular dynamics. We hope that our work will stimulate further theoretical analysis.

Conclusions

We have presented a comprehensive study of water wettability on graphene suspended on various nanotextured surfaces. By varying the fraction of solid area of the support we were able, for the first time, to measure the water contact angle on a single graphene sheet almost completely suspended on air or supported by water. Through physical and chemical substrates engineering, we were also able to study the substrate dependence of graphene's wettability to an unprecedented extent. Altogether, these results indicate that the contact angle of water on supported graphene is dictated almost exclusively by (long range attractive and short range repulsive) liquid-graphene interactions. Only ~20% of the long-range interactions between the liquid and the substrate are transmitted through graphene. Our findings shed new lights on the role of liquid-solid microscopic interaction on macroscopic quantities such as the contact angle. They are also relevant to many technological applications of graphene including advanced coatings[36–38] and water filtration membranes[39].

Methods

Substrate functionalization. The nanopatterned and flat substrates were degreased by sonication in successive baths of acetone, isopropyl alcohol and water. The samples were then immersed in a 40 mL mixture of hydrogen peroxide and sulfuric acid (1:3 v/v) for 15 minutes, thoroughly rinsed with deionized water and dried with nitrogen. This surface treatment results in highly hydrophilic substrates.

In order to obtain the (super)hydrophobic substrates, the substrates were left overnight in a mixture of 10 mL hexadecane, 1 mL choloroform and 133 µL of 1H-1H-2H-2H-perfluorodecyltrichlorosilane (ABCR, Germany) under Ar atmosphere. The substrates were then rinsed in chloroform and dried with nitrogen.

Graphene transfer method. In our investigations we have used commercially-available graphene monolayers (Graphene Supermarket Inc. USA and Graphenea, SP) grown on copper surfaces by chemical vapor deposition (CVD). A ~1 cm^2 as-synthesized piece of graphene-coated copper foil is floated at the surface of a dilute aqueous solution of copper etchant ($(NH_4)_2S_2O_8$) with graphene exposed to air (see Fig. 2a). A large solution volume (100 mL) and low etchant concentration (10^{-2} M) were used to promote a slow, steady etch rate (<500 nm/h) necessary to prevent the fragmentation of the copper foil into sub-millimeter grains, which may tear and sink the floating graphene layer. After complete dissolution of the copper foil (48–72 h), the graphene monolayer is left floating intact at the liquid-air interface. Although this process is performed in cleanroom environment, adventitious contamination on CVD-grown graphene typically provides enough reflective contrast to see the monolayer floating on the etching solution with the naked eye. The floating graphene is then carefully scooped out onto a rinsing bath of deionized water using a glass slide pre-cleaned in a mixture of hydrogen peroxide and

sulfuric acid (1:3 by volume). After typically 15 minutes, the graphene layer is again scooped out of the rinsing bath using the final substrate. In the case of flat and patterned hydrophilic substrates, this step is greatly facilitated by the solution that wets the substrate completely. However, the deposition on hydrophobic substrates is more challenging because water spontaneously dewets these surfaces. We obviated this issue by adding a small amount of isopropanol (12% v/v) to the rinsing bath of distilled water thereby lowering the surface tension of the solution enough to induce complete wetting on the hydrophobic surfaces. After the transfer was completed, the samples were dried at room temperature.

Graphene cleaning procedure. Prior to any contact angle measurements, the samples were cleaned by annealing under a Ar/H_2 atmosphere. The samples were heated up to 350 °C following a ramp of 5 °C/min, under a argon flux of 300 sccm, and kept at this temperature during 4 hours with an additional flux of hydrogen (75 sccm). The oven was naturally cooled down to ambient temperature under Ar flux.

Sample characterization. The samples were first characterized using an optical microscope (Olympus BX60) and scanning electron microscope (FIB-SEM Zeiss 1540XB). Micro-Raman spectra were acquired on a Horiba Xplora-MV2000 spectrometer. AFM characterization were performed on a Multimode 8 AFM (Bruker) in Tapping mode using OTESPA cantilevers. The contact angle measurements were performed on a Kruss DSA100 goniometer following the procedure detailed in Supplementary Section SI4.

Wettability of HOPG. The wettability of HOPG was characterized using a $10 \times 10 \times 1$ mm HOPG (type ZYA) sample purchased from Scientec (France). The sample was exfoliated several times using a scotch tape until a flat surface was obtained. All measurements were performed on freshly exfoliated surfaces *i.e.* within 5 minutes after the last peeling. The obtained values were reproducible leading to $\theta_{HOPG,adv} = 62, 4° \pm 0, 9°$ and $\theta_{HOPG,rec} = 60, 2° \pm 1, 1°$.

When left overnight under ambient conditions, the contact angles drastically changed to reach $\theta_{HOPG,adv} = 90° \pm 1°, 6°$ and $\theta_{HOPG,rec} = 51, 2° \pm 1, 5°$. This evolution gives a large increase of hysteresis that can be associated to the adsorption of airborne contaminants, similar to the ones affecting measurements on graphene monolayers.

References

1. Soldano, C., Mahmood, A. & Dujardin, E. Production, properties and potential of graphene. *Carbon* **48,** 2127–2150 (2010).
2. Nine, M. J., Cole, M. A., Tran, D. N. H. & Losic, D. Graphene: a multipurpose material for protective coatings. *Journal of Materials Chemistry A* **3,** 12580–12602 (2015).
3. Rafiee, J. *et al.* Wetting transparency of graphene. *Nature Mat.* **11,** 217–222 (2012).
4. Shih, C.-J. *et al.* Breakdown in the Wetting Transparency of Graphene. *Phys. Rev. Lett.* **109,** 176101 (2012).
5. Raj, R., Maroo, S. C. & Wang, E. N. Wettability of Graphene. *Nano Lett.* **13,** 1509–1515 (2013).
6. Peng, S., Lohse, D. & Zhang, X. Microwetting of Supported Graphene on Hydrophobic Surfaces Revealed by Polymerized Interfacial Femtodroplets. *Langmuir* **30,** 10043–10049 (2014).
7. Parobek, D. & Liu, H. Wettability of graphene. *2D Mater.* **2,** 032001 (2015).
8. Bonn, D., Eggers, J., Indekeu, J., Meunier, J. & Rolley, E. Wetting and spreading. *Rev. Mod. Phys.* **81,** 739–805 (2009).
9. de Gennes, P. G. Wetting - Statics and Dynamics. *Rev. Mod. Phys.* **57,** 827–863 (1985).
10. Li, Z. *et al.* Effect of airborne contaminants on the wettability of supported graphene and graphite. *Nature Mat.* **12,** 925–931 (2013).
11. Kozbial, A. *et al.* Understanding the intrinsic water wettability of graphite. *Carbon* **74,** 218–225 (2014).
12. Martinez-Martin, D. *et al.* Atmospheric contaminants on graphitic surfaces. *Carbon* **61,** 33–39 (2013).
13. Voloshina, E., Usvyat, D., Schuetz, M., Dedkov, Y. & Paulus, B. On the physisorption of water on graphene: a CCSD(T) study. *Phys. Chem. Chem. Phys.* **13,** 12041–12047 (2011).
14. Ambrosetti, A. & Silvestrelli, P. L. Adsorption of Rare-Gas Atoms and Water on Graphite and Graphene by van der Waals-Corrected Density Functional Theory. *J. Phys. Chem. C* **115,** 3695–3702 (2011).
15. Kim, D., Pugno, N. M., Buehler, M. J. & Ryu, S. Solving the Controversy on the Wetting Transparency of Graphene. *Sci. Rep.* **5,** 15526 (2015).
16. Driskill, J., Vanzo, D., Bratko, D. & Luzar, A. Wetting transparency of graphene in water. *J. Chem. Phys.* **141,** 18C517 (2014).
17. Checco, A., Rahman, A. & Black, C. T. Robust Superhydrophobicity in Large-Area Nanostructured Surfaces Defined by Block-Copolymer Self Assembly. *Adv. Mat.* **26,** 886–891 (2014).
18. Li, X. *et al.* Large-Area Synthesis of High-Quality and Uniform Graphene Films on Copper Foils. *Science* **324,** 1312–1314 (2009).
19. Asadi, K. *et al.* Up-Scaling Graphene Electronics by Reproducible Metal-Graphene Contacts. *ACS Appl. Mater. Interfaces* **7,** 9429–9435 (2015).
20. Kim, K. S. *et al.* Large-scale pattern growth of graphene films for stretchable transparent electrodes. *Nature* **457,** 706–710 (2009).
21. Kobayashi, T. *et al.* Production of a 100-m-long high-quality graphene transparent conductive film by roll-to-roll chemical vapor deposition and transfer process. *Appl. Phys. Lett.* **102,** 023112 (2013).
22. Lin, Y.-C. *et al.* Graphene Annealing: How Clean Can It Be? *Nano Lett.* **12,** 414–419 (2012).
23. Wood, J. D. *et al.* Annealing free, clean graphene transfer using alternative polymer scaffolds. *Nanotechnology* **26,** 055302 (2015).
24. Reserbat-Plantey, A. *et al.* Strain Superlattices and Macroscale Suspension of Graphene Induced by Corrugated Substrates. *Nano Lett.* **14,** 5044–5051 (2014).
25. Ishigami, M., Chen, J. H., Cullen, W. G., Fuhrer, M. S. & Williams, E. D. Atomic structure of graphene on SiO_2. *Nano Lett.* **7,** 1643–1648 (2007).
26. Salehi-Khojin, A. *et al.* Polycrystalline Graphene Ribbons as Chemiresistors. *Adv. Mat.* **24,** 53–57 (2012).
27. Quéré, D. Wetting and roughness. *Annu. Rev. Mater. Res.* **38,** 71–99 (2008).
28. Cassie, A. B. D. & Baxter, S. Wettability of porous surfaces. *T. Faraday. Soc.* **40,** 0546–0550 (1944).
29. Py, C. *et al.* Capillary Origami: Spontaneous wrapping of a droplet with an elastic sheet. *Phys. Rev. Lett.* **98,** 156103 (2007).
30. Patra, N., Wang, B. & Kral, P. Nanodroplet Activated and Guided Folding of Graphene Nanostructures. *Nano Lett.* **9,** 3766–3771 (2009).
31. Israelachvili, J. *Intermolecular and Surface Forces.* (Academic Press, 1992).
32. Shih, C.-J., Strano, M. S. & Blankschtein, D. Wetting translucency of graphene. *Nature Mat.* **12,** 866–869 (2013).
33. Leroy, F., Liu, S. & Zhang, J. Parametrizing Nonbonded Interactions from Wetting Experiments via the Work of Adhesion: Example of Water on Graphene Surfaces. *J. Phys. Chem. C* **119,** 28470–28481 (2015).

34. Sforzini, J. *et al.* Approaching Truly Freestanding Graphene: The Structure of Hydrogen-Intercalated Graphene on 6H-SiC(0001). *Phys. Rev. Lett.* **114,** 106804 (2015).
35. Britnell, L. *et al.* Field-Effect Tunneling Transistor Based on Vertical Graphene Heterostructures. *Science* **335,** 947–950 (2012).
36. Chen, S. *et al.* Oxidation Resistance of Graphene-Coated Cu and Cu/Ni Alloy. *ACS Nano* **5,** 1321–1327 (2011).
37. Berman, D., Erdemir, A. & Sumant, A. V. Few layer graphene to reduce wear and friction on sliding steel surfaces. *Carbon* **54,** 454–459 (2013).
38. Coraux, J. *et al.* Air-Protected Epitaxial Graphene/Ferromagnet Hybrids Prepared by Chemical Vapor Deposition and Intercalation. *J. Phys. Chem. Lett.* **3,** 2059–2063 (2012).
39. O'Hern, S. C. *et al.* Selective Ionic Transport through Tunable Subnanometer Pores in Single-Layer Graphene Membranes. *Nano Lett.* **14,** 1234–1241 (2014).

Acknowledgements

We thank Xavier Bouju (CEMES-CNRS) and Mathias Rapacioli (LCPQ, Toulouse) for fruitful discussions. This study has been partially supported through the Laboratory of Excellence NEXT (grant n° ANR-10-LABX-0037) in the framework of the "Programme des Investissements d'Avenir". M.N. acknowledges the government of Andorra for a PhD fellowship. A.C. acknowledges financial support by NEXT through a Senior Guest Fellowship. Research carried at Brookhaven National Laboratory is supported by the U.S. Department of Energy, Office of Basic Energy Sciences, under Contract No. DE-SC0012704 and used resources of the Center for Functional Nanomaterials, which is a U.S. DOE Office of Science Facility.

Author Contributions

T.O. and A.C. designed the research. V.T., T.O. and A.C. fabricated the suspended graphene samples and performed contact angle measurements. M.N. and E.D. developed the graphene transfer, annealing and characterization methods. C.T.B. and A.R. fabricated the nanopatterned substrates. T.O., A.C. and E.D. drafted the manuscript. All authors reviewed and approved the manuscript.

Additional Information

Supplementary information accompanies this paper at http://www.nature.com/srep

Competing financial interests: The authors declare no competing financial interests.

How to cite this article: Ondarçuhu, T. *et al.* Wettability of partially suspended graphene. *Sci. Rep.* **6**, 24237; doi: 10.1038/srep24237 (2016).

Supplementary information

Wettability of partially suspended graphene

Thierry Ondarçuhu, [1*] Vincent Thomas, [1] Marc Nuñez, [1] Erik Dujardin, [1] Atikur Rahman, [2]

Charles T. Black,[2] and Antonio Checco, [3*]

[1] *Nanosciences group, CEMES-CNRS, 29 rue Jeanne Marvig, 31055 TOULOUSE (France)*

[2] *Center for Functional Nanomaterials, Brookhaven National Laboratory, Upton, NY , 11973 (USA)*

[3] *Condensed Matter Physics and Materials Science Department, Brookhaven National Laboratory, Upton, NY 11973 (USA)*

Supplementary Information

SI1: Graphene wrinkles formation

The transfer method used in this study leads to the formation of wrinkled graphene layers. In order to get insight in the formation of the folds, we observed graphene layers during all steps of the process. The pattern of folds is not correlated to the grain boundaries of the copper foil supporting the graphene layer at the initial stage. Moreover, PMMA-assisted transfer of the same graphene sample did not show the presence of any wrinkle, indicating that the folding occurs latter in the process. Indeed, it was observed that the graphene layer is already folded when lying at the liquid interface (see Fig SI1) showing that folds do not result from the drying of the liquid layer on the substrate. The wrinkling therefore occurs at the liquid interface, due to surface tension effects when the copper foil is etched away. Indeed, the first millimeter in the periphery of the graphene layer is fully crumpled which is useful to visualize the graphene sheet floating at the liquid interface.

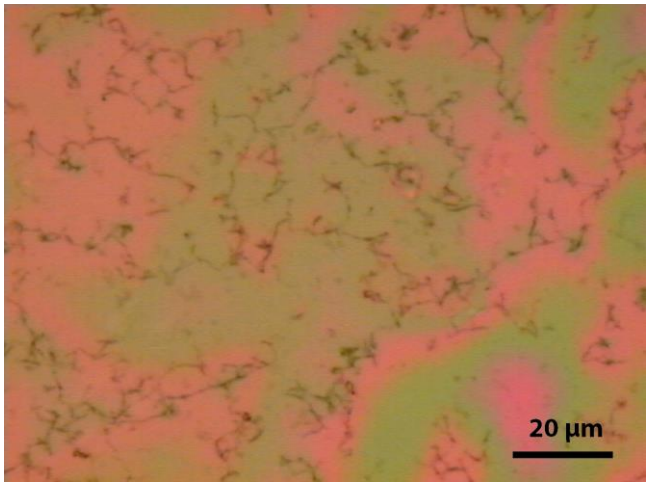

Fig SI1: Optical micrograph of a graphene layer floating on a liquid film above a hydrophilic flat SiO_2 substrate. Colors are due to interference fringes in the thin liquid film. Black features are folds of the graphene layer.

SI2: Characterization of suspended graphene layers

The partially supported graphene layers were characterized by SEM and AFM. The patterns of folds present the same characteristics as the ones observed on flat substrates. They are clearly evidenced in the images (see Fig. SI2a, SI2c and SI2d), together with the holes in the layer. The main difference with flat substrates lies in the occasional presence, on patterned substrates, of short cracks that propagate following the paths between posts (see Fig. SI2b). For substrates with conical texture ($\phi < 15\%$), the density of defects may increase significantly and reach 8% for the sharper surface used ($\phi = 6\ \%$) as shown in Fig. SI2e.

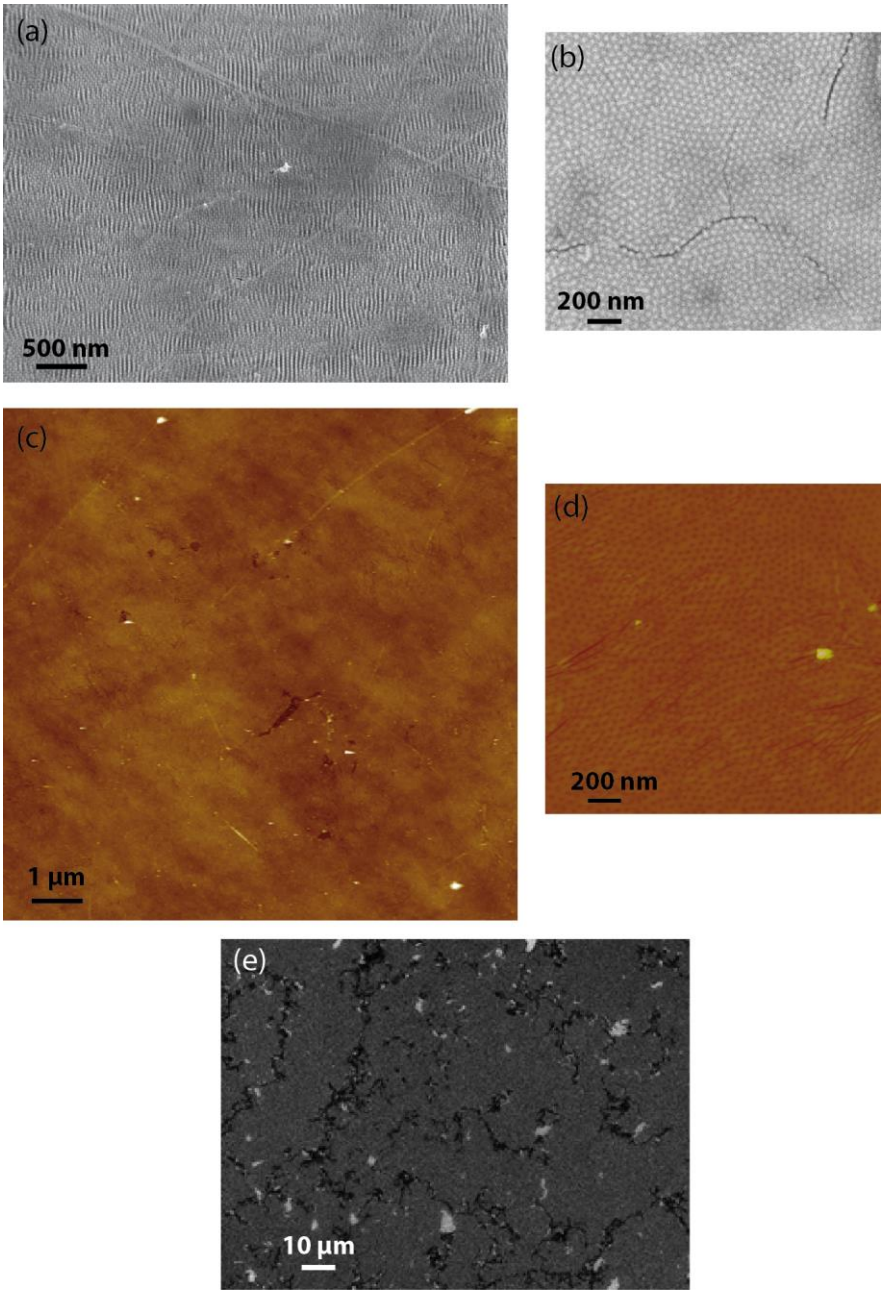

Fig SI2: (a) SEM image of a graphene monolayer deposited on a substrate with nailhead posts (for better contrast the sample was tilted by54°). (b) SEM image on an area where the layer presents some cracks following the pillars pattern. (c) Large scale AFM image of a partially suspended monolayer where holes and folds are clearly visible. (d) Zoom on a flat area. (e) SEM image of a graphene layer deposited on a substrate with conical texture ($\phi = 6\%$). The contrast was enhanced to visualize the holes in the layer which appear bright in the image and represents 8% of the total area.

SI3: Annealing procedure

Prior to any contact angle measurements, the samples were cleaned by annealing under a Ar/H_2 atmosphere. The samples were heated up to 350 °C following a ramp of 5°C/min, under a argon flux of 300 sccm, and kept at this temperature during 4 hours with an additional flux of hydrogen (75 sccm). The oven was naturally cooled down to ambient temperature under Ar flux. Even though the optical imaging reveals the removal of some black particles already present on the copper foil, the effect of the annealing process on the graphene quality was further assessed by high resolution TEM (HR-TEM) on graphene layers deposited using the resist-free procedure on TEM grids. The images before and after annealing are reported on Fig. SI3a-b together with diffraction patterns. No structure is visible before annealing whereas the crystalline structure of the graphene clearly shows up in the TEM micrographs and diffraction after treatment, demonstrating the efficiency of the Ar/H_2 annealing.

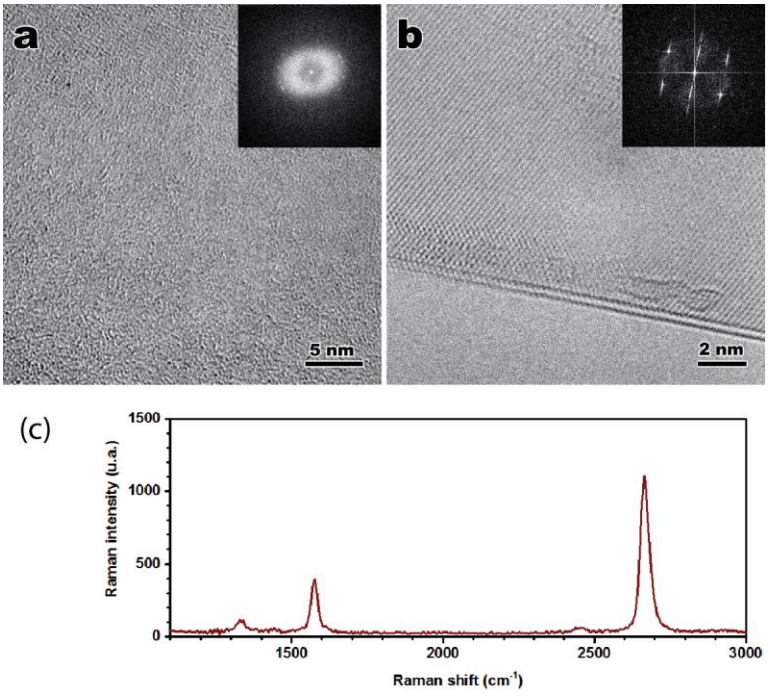

Fig SI3: HRTEM image and diffraction pattern (inset) of a graphene monolayer: (a) before annealing; (b) after annealing; (c) Raman spectrum of a supported graphene layer.

Micro-Raman spectra were acquired on a Horiba Xplora-MV2000 spectrometer in a 1-μm focal spot area exempt of visible wrinkle (Figure SI3c). Two intense peaks are recorded at 1580 cm^{-1} and 2670 cm^{-1} that correspond to the G and 2D bands of graphene respectively. Two weaker peaks at 1330 cm^{-1} and 2450 cm^{-1} are the first order D band and the second order D+D" band,[1,2] which characterize defects in the layer. The areal ratio of the 2D and G bands ($\frac{A_{2D}}{A_G} \sim 4-5$) together with the single Lorentzian shape of the 2D band are strong indications of a single monolayer. As expected, micro-Raman spectra measured on wrinkles exhibit a much more intense D band due to a higher density of defects in these regions.

SI4: Protocol for contact angle measurements on supported graphene layers

The contact angle measurements were performed on a Kruss DSA100 goniometer. In order to optimize the protocol to achieve contact angle measurements of water on graphene layers, we transferred on SiO_2/Si flat samples, graphene layers from three different commercially available graphene sources (two from Graphene Supermarket Inc. USA and one from Graphenea, SP) grown on copper surfaces by chemical vapor deposition (CVD). After transfer the samples were cleaned using the annealing procedure described in the previous section.

Advancing and receding contact angles were measured on several graphene regions, immediately after the reductive annealing and for a few hours afterwards (see Figure SI4) in order to probe the dynamics of airborne contaminants re-adsorption. The results show no influence of the graphene source. Importantly, the measurements on flat substrates reveal an increase of the contact angle with time, in agreement with recent reports.[3,4] In particular, the advancing contact angle increases from 68° ± 1 ° reaching a plateau at 85° ± 2° when exposed to ambient air, in agreement with the results of Li *et al.*.[3] However, we have found that the wettability change occurs on a time scale of ca. 5 hours rather than 1h, as reported in ref. 2a, provided that the cleaned samples are kept under nitrogen atmosphere at all time. In agreement with recent AFM force measurements,[5] this evolution of the advancing angle is attributed to the decrease in effective surface energy as water and airborne hydrocarbon contaminants adsorb on graphene. For these reasons, all the contact measurements reported here were performed within ten minutes from the end of annealing process. Conversely, the receding contact angle was found not to vary significantly (θ_{rec}= 45° ± 2°) after the annealing process, suggesting that this quantity is dominated by pinning of the receding contact line on anchoring defects,[6] which are present after the transfer of graphene but do not evolve in time.

Interestingly, the receding contact angle found here is identical to the one reported in ref. 2a on wrinkle-free graphene obtained by PMMA-assisted transfer, thus indicating that the wrinkles generated by the resist-free transfer method do not modify significantly the anchoring of water droplets on graphene.

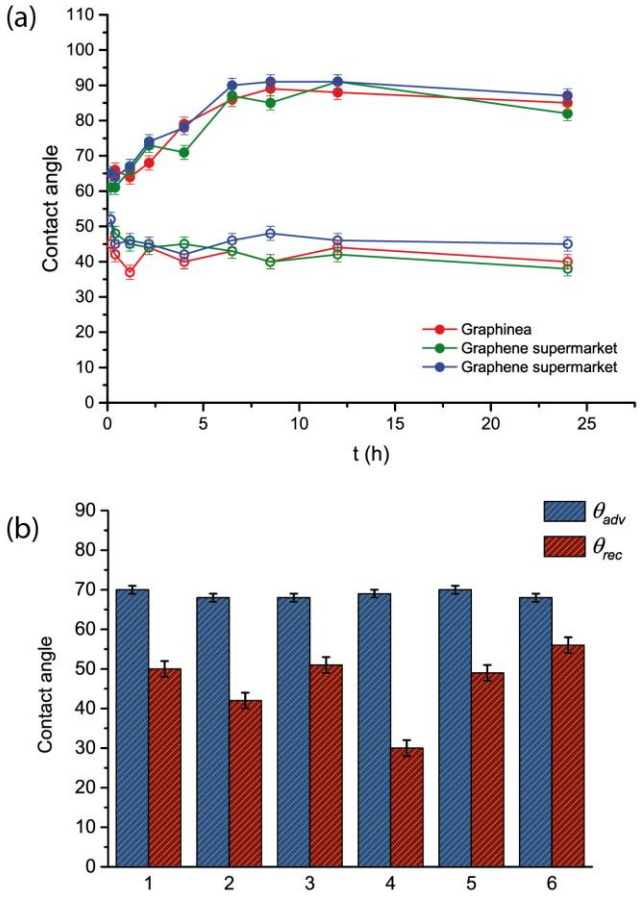

Fig SI4: (a) Advancing (filled circles) and receding (empty circles) water contact angles of supported graphene monolayers from three different sources, as a function of the time after the annealing process. (b) Advancing (blue bars) and receding (red bars) water contact angles of 6 different supported Graphene Supermarket graphene monolayers.

The repeatability of the contact angle measurements was checked by performing identical experiments on six different layers transferred on flat Si/SiO_2 surfaces pre-cleaned by sulfuric

acid and hydrogen peroxide solution. The results show that the value of the advancing contact angle is highly reproducible (standard deviation < 1°) while receding contact angle values are more spread (s.d. > 9°). This is also consistent with the conclusions of Raj *et al.*[6] and suggests that the advancing contact angle provides a more reliable measure of the intrinsic wettability of graphene compared to the receding angle, which is more influenced by monolayer defects. For this reason, we only report advancing contact angles measurements.

SI5: Influence of defects

In order to assess the influence of defects in the graphene layer, we considered a graphene layer with a contact angle θ_G assumed independent of the underlying substrate and with a density of defects (holes) Φ_d. The contact angle of the defective layer can then be calculated using a Cassie-Baxter equation using the substrate contact angle θ_S for the defects. It reads

$$\cos\theta = (1 - \Phi_d)\cos\theta_G + \Phi_d \cos\theta_S \qquad (1)$$

On Fig. SI5, the expression given by Eq. (1) is plotted for two different density of defects namely Φ_d=2% and 8%. As expected the influence of defects increases with defects density. For $\Phi_d = 2\%$ which corresponds to the majority of samples studied, the variation of contact angle is negligible. On sharp textures, the density of defects increases up to $\Phi_d = 8\%$ which may explain part of the evolution of contact angle measured experimentally.

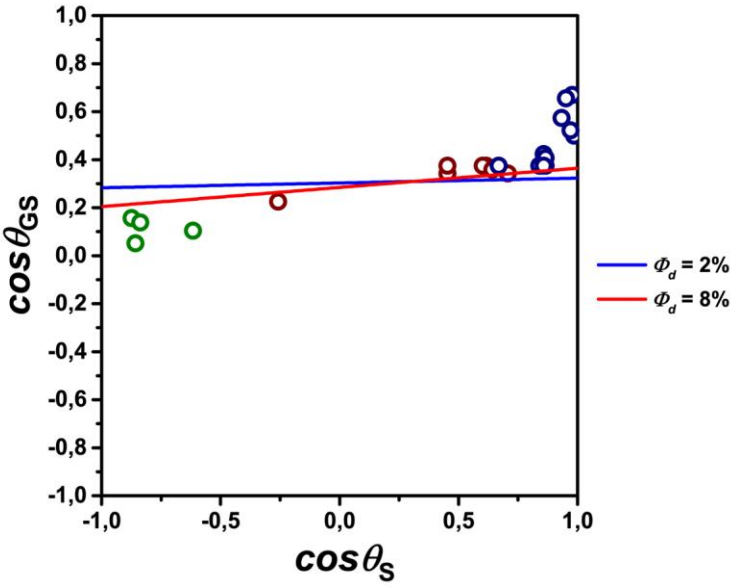

Figure SI5. Plot of the experimental data (dots) and of the predicted curves for three different densities of defects (Eq. (1)).

The variation of contact angle $\Delta\theta_d$ between graphene suspended on water ($\cos\theta_S = 1$) and air ($\cos\theta_S = -1$) associated to the only presence of defects can be estimated using Eq. (1). It reads:

$$\Delta\theta_d = -\frac{2\phi_d}{\sin\theta} \quad (2)$$

It gives $\Delta\theta_d \approx -3°$ for $\Phi_d = 2$ % and $\Delta\theta_d \approx -10°$ for $\Phi_d = 8$ % which can explain only a fraction of the $\Delta\theta_{GS} \approx -24°$ value measured experimentally.

SI6: Wettability of multilayer graphene and graphite

In a rough approximation, the wettability of multilayer graphene can be estimated graphically Indeed, the contact angle on n+1 layers can be determined from the contact angle on n layers using the $cos\theta_{GS} = f(cos\theta_S)$ relation deduced experimentally. This leads to $cos\theta_{(n+1)GS} = f(cos\theta_{nGS})$. $cos\theta_{(n+1)GS}$ can then be used to compute $cos\theta_{(n+2)GS}$. This can be simply obtained graphically using the diagonal of the graph as shown on Figure SI6a starting from a suspended single monolayer. The same could be obtained for multilayer graphene floating on water, starting from $cos\theta_S = 1$, or from any situation. In Figure SI6b are reported the contact angles as a function of the number of layers in both situations. It shows that both values converges rapidly towards a value which corresponds to the contact angle on HOPG i.e the stack of an infinite number of graphene layers. This convergence is rather fast since the contact angle value for a 3-layers (4-layers) configuration approaches the one of HOPG value within 0,7° (0,14°), respectively.

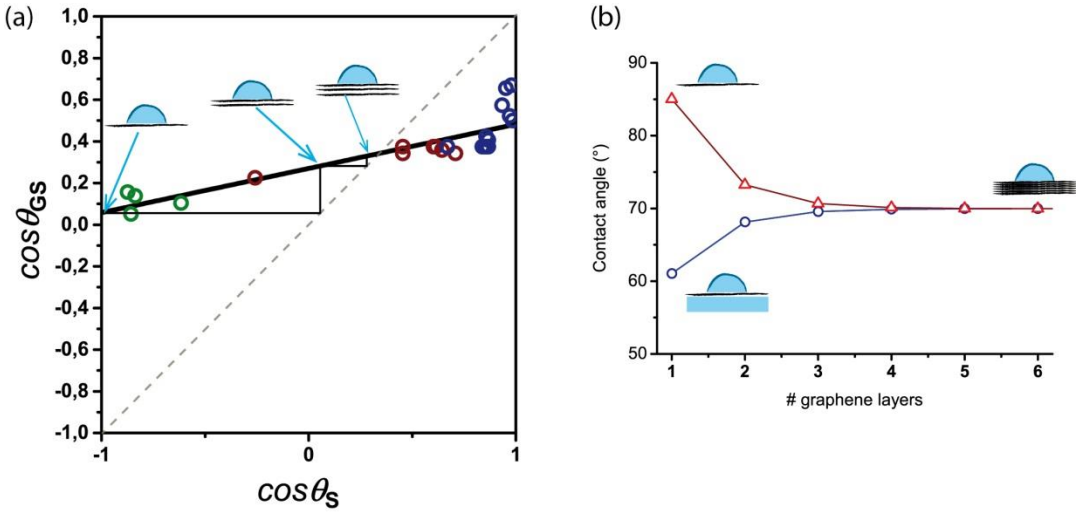

Figure SI6. (a) Graphical construction of the contact angle on multi-layers graphene starting form a single suspended graphene layer. (b) Contact angle of water as a function of the number of graphene layers suspended in red triangles and floating on water in blue circles.

References

1. May, P. *et al.* Signature of the two-dimensional phonon dispersion in graphene probed by double-resonant Raman scattering. *Phys. Rev. B* **87**, 075402, (2013).
2. Narula, R. & Reich, S. Probing LO phonons of graphene under tension via the 2D ' Raman mode. *Phys. Rev. B* **87**, 115424, (2013).
3. Li, Z. *et al.* Effect of airborne contaminants on the wettability of supported graphene and graphite. *Nature Mat.* **12**, 925-931, (2013).
4. Kozbial, A. *et al.* Understanding the intrinsic water wettability of graphite. *Carbon* **74**, 218-225, (2014).
5. Lai, C.-Y. *et al.* A nanoscopic approach to studying evolution in graphene wettability. *Carbon* **80**, 784-792, (2014).
6. Raj, R., Maroo, S. C. & Wang, E. N. Wettability of Graphene. *Nano Lett.* **13**, 1509-1515, (2013).